AIAA JOURNAL
Vol. 45, No. 2, February 2007

Wake Vortex Control Using Static Segmented Gurney Flaps

Claude G. Matalanis* and John K. Eaton†
Stanford University, Stanford, California 94305

DOI: 10.2514/1.25956

A study to assess the potential for using static segmented Gurney flaps, also known as miniature trailing edge effectors, for active wake vortex alleviation is conducted using a half-span model wing with NACA 0012 shape and an aspect ratio of 4.1. All tests are performed with the wing at an 8.9 deg angle of attack and chord-based Reynolds number around 350,000. The wing is equipped with an array of 13 miniature trailing edge effector pairs. Each miniature trailing edge effector has a flap that in the neutral position rests behind the blunt trailing edge of the wing, and in the down position extends 0.015 chord lengths perpendicular to the freestream on the pressure side of the wing. Measurements of section lift coefficient are made using pressure taps to assess the effect of various miniature trailing edge effector configurations on the spanwise lift distribution. Particle image velocimetry and five-hole probe measurements are made on the trailing vortex to assess the steady-state effects of different flap configurations. It is found that the miniature trailing edge effector configurations with a large fraction of the span actuated down are able to deflect the vortex predominantly in the lift direction, whereas miniature trailing edge effector configurations with a small fraction of the span actuated down are able to deflect the vortex in both the spanwise and lift direction. A maximum spanwise deflection of 0.041 chord lengths is possible while nearly conserving total lift. These results suggest that certain miniature trailing edge effector configurations, if varied in time, may be useful for wake alleviation.

Nomenclature

a	=	wing half-span
a_{down}	=	spanwise length of MiTEs in down position
AR	=	wing aspect ratio $(2a/c)$
c	=	wing chord length
C_L	=	total lift coefficient
C_l	=	section lift coefficient
C_p	=	pressure coefficient
U_∞	=	freestream velocity
V, W	=	mean velocity in (Y, Z) direction
X, Y, Z	=	physical coordinate system measured from wing root trailing edge
X'	=	streamwise length measured along wing chord line
Y_{flap}	=	spanwise location of centroid of MiTEs in down position
$\Delta Y, \Delta Z$	=	coordinate system centered on neutral case vortex location
ω	=	streamwise vorticity

I. Introduction

GURNEY flaps are small flaps oriented perpendicular to the freestream at the trailing edge of an airfoil or wing which can increase the lift considerably with only a small drag penalty. Previous research has shown that they accomplish this by effectively changing the shape of the airfoil and increasing the circulation generated by it [1–8]. The drag increase has been found to be small as long as the flap remains inside the airfoil boundary layer. Research has shown that Gurney flaps are effective when applied to single-element airfoils as well as multielement airfoils in high lift configurations [9,10]. Miniature trailing edge effectors (MiTEs) are segmented, independent Gurney flaps that have an analogous effect local to their spanwise position. Recent work has shown that the effect of a MiTE on the pressure distribution of a wing is strongest at the spanwise position of that particular MiTE, and that the effect fades away quickly moving in either spanwise direction [11–13].

MiTEs have already shown great potential in alleviating aerodynamic problems such as flutter [14]. Using an array of MiTEs in a closed-loop control configuration, it was shown that the flutter speed of a test wing could be increased significantly. The potential for using MiTEs for conventional control of an uninhabited air vehicle was also examined.

MiTEs also show potential in solving the wake vortex hazard problem where the goal is to introduce vortex perturbations while holding the total lift of the wing nearly constant. Because the effect of a MiTE or group of neighboring MiTEs is concentrated at the actuated span, MiTEs allow for some control over not only the total lift experienced by the wing but also the shape of the spanwise lift distribution. Changes in the loading distribution are likely to cause changes in the downstream evolution of the vortex.

The wake vortex hazard has received considerable attention over the past 35 years, and with the increase in air traffic that is likely to take place, as well as the introduction of another 400+ passenger commercial airliner, the problem is becoming more urgent [15–17]. Large aircraft that produce high lift also produce large, coherent vortices that can persist in the wake for long times after the aircraft has passed. This can pose a serious threat to following aircraft, especially when the follower is significantly smaller. Several accidents have been attributed indirectly to this problem. One approach to solving the problem is by wake alleviation. The idea is to, by some means, render the wake of high lift aircraft benign to following aircraft in less time than the wake would normally require.

In general, wake alleviation strategies fall into two categories: active and passive. Passive strategies rely upon a static wing or aircraft configuration that would result in a less hazardous or nonhazardous wake. Many ideas have been studied, including turbulence injection by blowing [18], the use of conventional flaps [19], the addition of spoilers to aircraft wings [20], the addition of triangular flaps to wing tips [21–23], wings with notched lift distributions [24], and the addition of tail wings that produce vorticity of opposite sign [25]. Active strategies rely upon introducing some time-dependent disturbance to the flow to excite an instability in the wake, and accelerate the destruction of the trailing vortices. Although trailing vortices tend to be quite stable, several

Received 16 June 2006; revision received 21 August 2006; accepted for publication 22 August 2006.

*Graduate Student, Mechanical Engineering, Building 500-501R. Student Member AIAA.

†Professor, Mechanical Engineering, Building 500-501F. Senior Member AIAA.

instability mechanisms are known to exist for a single pair of vortices and other vortex configurations[26–29].

To be practically applicable, a successful wake alleviation scheme should keep the lift experienced by the wing or aircraft fairly constant. One way of doing this is to alter the shape of the spanwise lift distribution in time while holding the total lift constant. The concept of exciting vortex pair instability in this fashion is not new. The idea was proposed by Crow and Bate [30] as a means of exciting the instability that bears Crow's name. Bilanin and Widnall [31] performed a study using conventional flaps for this same purpose, sloshing a large fraction of the lift generated by the wings periodically inboard and outboard. Work has been done more recently suggesting that even small perturbations of this fashion can be useful when applied properly [28,29,32–34].

The overall objective of this work is to assess the potential of MiTEs for wake alleviation. We do this by applying an array of MiTEs across the entire span of a NACA 0012 wing. A key feature of MiTEs is that they can be rapidly actuated; however, for the purposes of this work, we limit our study to only static configurations. We vary both the amount of span that is actuated and the spanwise location of the actuation, and we measure the effect experienced by the wing in terms of the loading distribution, and how the trailing vortex created by the wing in the intermediate wake is affected. This study builds an understanding of the authority we may have over a trailing vortex using MiTEs and can be used as a guide towards designing an effective active scheme.

II. Experimental Apparatus

A. Wing and MiTEs

The half-span model used in this work consists of a wing that has an untapered NACA 0012 profile with a chord length c of 300 mm, and a half-span a of 619 mm (AR = 4.1). The half-span is measured from the root to the furthest spanwise point on the tip. The tip of the wing is rounded with a semicircle that has a radius of curvature that varies according to the thickness of the wing. The trailing edge of the wing is blunt with a thickness of $0.02c$. The wing was fabricated in two halves by computer numerical control machining of a polyurethane-based material. It is mounted directly to the bottom wall of the wind tunnel as shown in Fig. 1. For all of the experiments presented here, the wing is at an 8.9 deg angle of attack, and the Reynolds number based on chord length is around 350,000. This angle of attack was chosen to maximize lift while insuring fully attached flow. The solid blockage ratio in this configuration is roughly 7%.

The wing is equipped with an array of 26 newly designed MiTEs, each with a flap that has a span of $0.03a$, and extends perpendicular to the freestream a distance of $0.015c$. The bodies of the MiTEs comprise the final 7.7% of the wing trailing edge, and are shaped to be consistent with the NACA 0012 shape. A schematic representation of the airfoil cross section and a MiTE are shown in Fig. 2. Each MiTE has two possible states, "neutral" and "down," the MiTEs are always commanded in pairs (the entire half-span comprises 13 MiTE pairs), and between each neighboring MiTE there is a spanwise gap of 2.7 mm. In the neutral position, the flap sits immediately behind the blunt trailing edge and maintains the symmetry of the airfoil. In the down position, the flap extends perpendicular to the freestream on the pressure side of the wing. A picture of the wing trailing edge with four MiTEs in the down position is shown in Fig. 3.

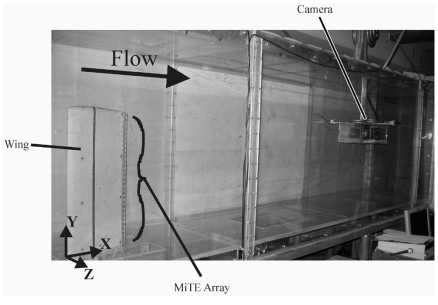

Fig. 1 The Stanford Flow Control Wind Tunnel test section.

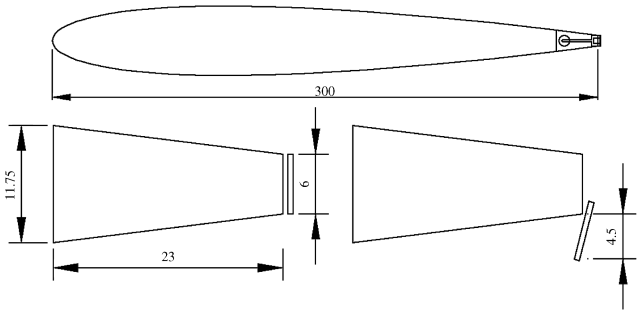

Fig. 2 Airfoil cross section and MiTE in X–Z plane. All dimensions in millimeters.

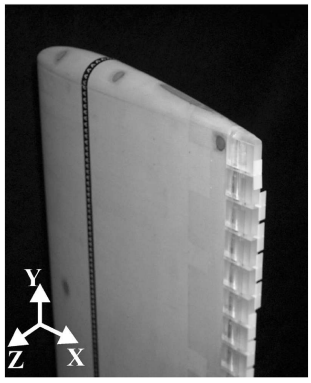

Fig. 3 Trailing edge of wing with four MiTEs actuated in down position.

The MiTEs are commanded by a computer that sends signals to a circuit that relays a constant voltage signal from a power supply to the desired MiTEs. The MiTEs remain in the desired static condition for the duration of the test.

B. Measurement Apparatus

The wing equipped with the array of MiTEs is mounted in the Stanford Flow Control Wind Tunnel as shown in Fig. 1. The tunnel is closed-loop and operates at atmospheric conditions with a maximum velocity of 22 m/s. The test section is 91 cm high, 61 cm wide, and 3.7 m long. The wing is mounted directly onto the bottom wall of the tunnel (no splitter plate) with the leading edge roughly 45 cm past the beginning of the test section where the boundary layer height should be less than 2 cm.

The wing is equipped with 217 0.635 mm diameter pressure taps for measuring the spanwise loading distribution as shown in Fig. 4. Seven rows of pressure taps are cosine spaced across the half-span of the wing to achieve better resolution near the tip where the section lift changes more with respect to spanwise location. Each row consists of 31 taps distributed chordwise across the pressure and suction sides of the wing. The taps are more densely spaced closer to the leading edge to improve resolution where the variation is more severe. One differential pressure transducer with a Scanivalve pressure-switching system is used to measure the pressure at each tap.

Velocity measurements are performed in the intermediate wake ($2.8 < X/c < 4.9$) using particle image velocimetry (PIV) to obtain high-resolution data in the vortex core and five-hole probe measurements to obtain low-resolution data over a much larger domain. The PIV measurement apparatus is shown schematically in Fig. 5. The flow is seeded using a commercial fog generator placed at the very end of the tunnel test section, and illuminated using a dual head Nd:YAG laser capable of 400 mJ/pulse. The laser sheet is oriented perpendicular to the freestream, and the sheet thickness is 2.5 mm. The region measured by PIV in all cases is 4.5 cm long in the

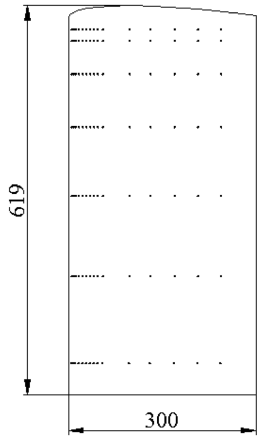

Fig. 4 Pressure tap locations (same on pressure and suction sides).

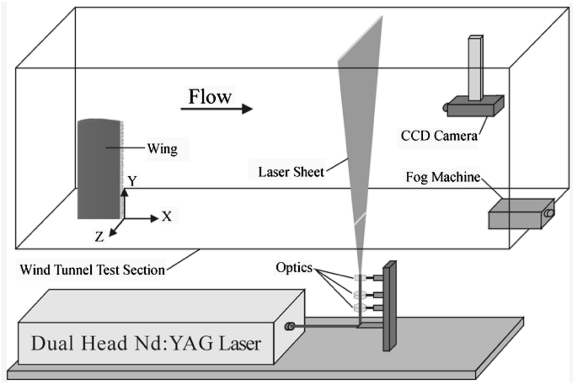

Fig. 5 Schematic representation of the experimental apparatus.

spanwise direction and 6 cm long in the lift direction. Image pairs are captured using a CCD camera mounted inside the wind tunnel downstream of the illuminated region such that the front of the camera is 0.75 m behind the laser sheet and upstream of the fog machine. Potential flow analysis indicated that the presence of the camera in the flow would have a negligible effect on the measurements, and this was confirmed by five-hole probe measurements done with and without the camera in the tunnel. The same was true for the fog machine. The changes observed were smaller than the cited uncertainties. Cross-correlation PIV is used to process the images and calculate the tangential velocities of the trailing vortex. For all of the PIV measurements, 500 image pairs are collected for each configuration. Measurements are taken at three positions behind the wing, $X/c = 2.8$, 3.8, and 4.9. According to the estimates given by Spreiter and Sacks [35], the vortex should be fully rolled up at a distance $X/c = 2.75$.

Five-hole probe measurements are performed at the $X/c = 4.9$ streamwise location. Three components of velocity are measured over a square region 20 cm by 20 cm large using a two-component (Y, Z) traverse mounted on top of the tunnel test section.

There are two coordinate systems used to present the data. The physical coordinate system, denoted by X, Y, and Z, is measured from an origin fixed at the location of the root trailing edge of the wing when the wing is at a zero angle of attack. We also use a vortex centered coordinate system denoted by ΔY and ΔZ (the streamwise direction X is the same in both coordinate systems). The $(\Delta Y, \Delta Z)$ origin is placed at the center location of the wing tip vortex produced with all the flaps in the neutral position.

The emphasis in all of our results is on comparing the effects of various flap configurations to one another. Thus, the uncertainties cited on all measured quantities account only for sources that would cause differences between the various cases. Bias errors that are the same for all cases are irrelevant, and are not included. All of the cited uncertainties were verified by repeatability tests. Furthermore, no attempt is made to correct any result to account for the tunnel walls as this constitutes another bias error.

The uncertainties in C_p and C_l are highest closest to the root. At $Y/a = 0.081$, accounting for statistical uncertainty, transducer drift, and uncertainty in angle of attack, the total uncertainties in C_p and C_l are ± 0.0090 and ± 0.0045, respectively. Based on these uncertainties, the uncertainty in C_L is ± 0.0031. For the PIV measurements, accounting for statistical uncertainty, and the uncertainty in angle of attack and freestream velocity, the total uncertainty in velocity is $\pm 0.81\%$ of U_∞, and the total uncertainty in $\omega c/U_\infty$ is ± 3.4. For the mean vortex center location, which is calculated using PIV data, the uncertainty calculation that proved to be most conservative was the repeatability in the measurement, ± 0.3 mm. There are likely several very small sources of error that are impossible to quantify making the repeatability the best estimate of the uncertainty. Finally, the total uncertainty in velocity as measured by the five-hole probe is $\pm 0.95\%$ of U_∞ for the V and W components and $\pm 0.73\%$ of U_∞ for the U component. This accounts for statistical uncertainty, uncertainty in angle of attack, and uncertainty in the probe location. Transducer drift was eliminated by frequently readjusting the offsets.

III. Results and Discussion

A. Spanwise Loading Distribution

A series of experiments was conducted to assess the influence that the MiTEs have upon the spanwise loading distribution of the wing. For all of the configurations examined, all MiTEs in the down position form a continuous group, i.e., no down MiTEs are ever separated by neutral ones. We vary two parameters, namely, a_{down}/a, which is the spanwise fraction of the wing with MiTEs in the down position, and Y_{flap}/a, which is the nondimensional spanwise centroid of the portion of the wing with MiTEs in the down position. These parameters are illustrated in Fig. 6.

Figure 7 is a plot of the pressure coefficient along the chord at the spanwise location closest to the root $(Y/a = 0.081)$ where the flow is essentially two-dimensional, i.e., spanwise variations are very small. Both the neutral case $(a_{\text{down}}/a = 0)$ and full span down case $(a_{\text{down}}/a = 0.865, Y_{\text{flap}}/a = 0.487)$ are shown. It is apparent that the effect of the MiTEs is felt along the entire chord line on both the pressure and suction sides of the wing. This is consistent with what other researchers have found [4,6]. Gurney flaps, or in our case, MiTEs, alter the effective shape of the wing in a way that increases the circulation generated about the airfoil section. The additional circulation effects an increase in lift that is distributed chordwise along the entire airfoil. The MiTEs do not bear very much of the additional load by themselves, which is an advantageous feature that helps to mitigate any increase in pitching moment they might cause.

For the full span down case, the total lift produced by the wing is increased by roughly 12.30%. The effect upon the pressure coefficient at each spanwise location is analogous to the location shown in Fig. 7. The entire spanwise loading distribution is shown in Fig. 8 for the neutral and full span down cases. The increment in section lift coefficient, C_l, caused by the array of MiTEs is not a constant across the span, but instead, the increase in C_l is always a fraction between 11.2 and 13.0% of the neutral case C_l.

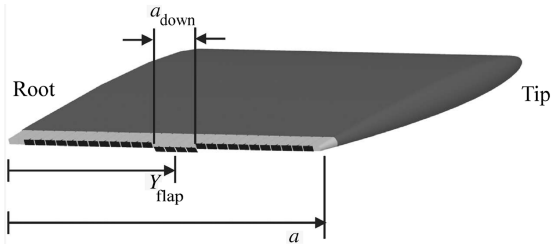

Fig. 6 Sketch of the wing and MiTEs.

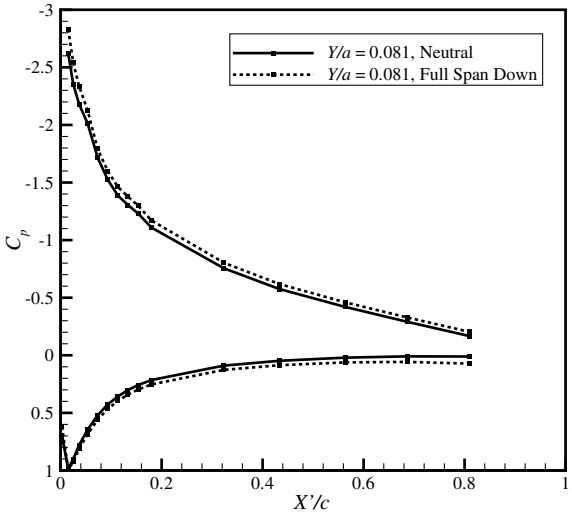

Fig. 7 The streamwise pressure coefficient distribution at $Y/a = 0.081$. The uncertainty in C_p is smaller than the symbol size.

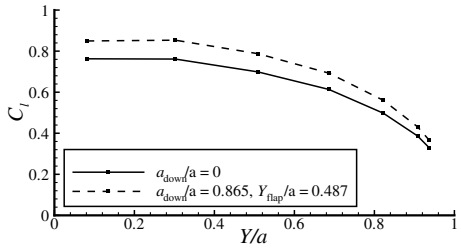

Fig. 8 Spanwise loading distribution. The uncertainty in C_l is smaller than the symbol size.

We consider now several other MiTE actuation configurations whose pressure profiles are shown in Figs. 9 and 10. First, we consider several configurations where a_{down}/a is relatively large. In Fig. 9a, we essentially divide the wing into two halves where one half is held in the down position, and the other is in the neutral position (amounts are not at even fractions due to the discrete location of the flaps). When the root half is in the down position ($Y_{\text{flap}}/a = 0.253$), the portion of the lift curve towards the root experiences the greatest increment in lift, and as we move towards the tip, the effect fades away. Note that the effect is still felt at the spanwise station closest to the tip, but it is significantly smaller. For the case where the tip half of the wing is in the down position ($Y_{\text{flap}}/a = 0.687$), we see the same effect in reverse. Here, the lift increment is greatest at the tip and drops off as we move towards the root. We find also that superposing the increments measured in these two cases produces the same increment that was produced by the full span down case to within 0.45% of the full span down distribution.

Figure 9b shows similar results, this time dividing the wing roughly into thirds. Again, the effect is concentrated at the spanwise

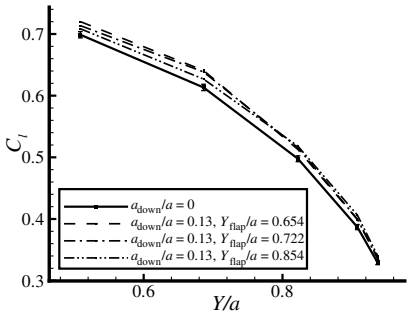

Fig. 10 Spanwise loading distribution near the tip. Uncertainty bars shown on the neutral case.

location with MiTEs down. The superposition of these three increments also roughly produces the full span down increment.

This apparent quasi-linearity in the flap effectiveness has been noted by other researchers [7,8,13]. The important aspect to note regarding these large a_{down}/a cases is that the increment in lift coefficient caused by the MiTEs is a function of both the amount of span that is actuated as well as the location of the actuated span.

In Fig. 10, we examine the influence upon the spanwise loading distribution for three cases where only four flaps are in the down position ($a_{\text{down}}/a = 0.13$) where we only consider values of Y_{flap}/a near the tip. These are locations most likely to be used for vortex control applications. Pressure data were not taken at the two spanwise stations closest to the root. We see the same basic trend that we noted in the previous cases. The $Y_{\text{flap}}/a = 0.654$ case causes the largest root increment (amongst these three cases), whereas the $Y_{\text{flap}}/a = 0.854$ case causes the largest increment near the tip.

Table 1 shows the change in total lift for each configuration as a percentage of the neutral case total lift. Note that only locations where data are available are integrated. This may slightly overestimate the lift increments for $a_{\text{down}}/a = 0.13$ cases. Although the effect upon the total lift is not negligible, it is quite small. More important, the maximum difference in lift between the small a_{down}/a configurations is only 0.91%. Thus, an active flow control scheme that involves cycling between these static configurations would conserve the total lift on the wing rather well.

B. Wake Measurements

PIV and five-hole probe measurements were made to assess the steady-state wake effects associated with MiTE actuation. The resolution achieved by the PIV measurements using 50% overlap when processing the image pairs is about 0.7 mm, allowing us to very accurately locate the center of the vortex. The five-hole probe measurements, on the other hand, are taken with a resolution of 12.5 mm to efficiently examine a much larger domain. Figure 11 shows the ensemble averaged velocity and vorticity field for a typical PIV data set for the neutral case at $X/c = 4.9$. For visual clarity, every other vector in both directions is removed.

To establish a baseline, we first examine the PIV results for the full span down case ($a_{\text{down}}/a = 0.865$, $Y_{\text{flap}}/a = 0.487$) and compare them to the neutral case. To present a large amount of data in a

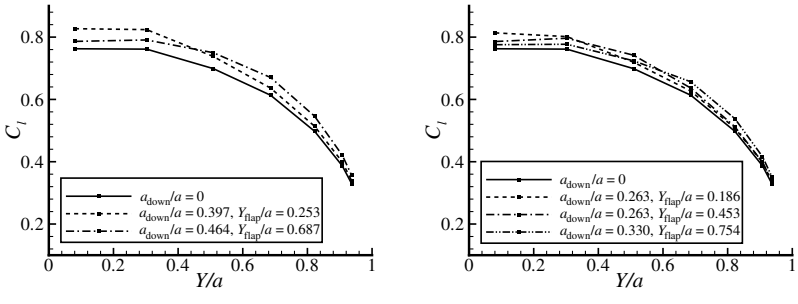

Fig. 9 Spanwise loading distributions. The uncertainty in C_l is less than or equal to the symbol size.

Table 1 Increment in lift compared to the neutral case

a_{down}/a	Y_{flap}/a	$\Delta C_L/C_L$
0.865	0.487	+12.30%
0.397	0.253	+6.12%
0.464	0.687	+6.32%
0.263	0.186	+3.96%
0.263	0.453	+4.34%
0.330	0.754	+4.09%
0.13	0.654	+3.62%
0.13	0.722	+3.35%
0.13	0.854	+2.71%

compact form, Fig. 12 gives the spanwise velocity and vorticity profiles across the center of the vortex. Each profile shown is the result of 500 image pairs for which we employ a center averaging technique to remove the effects of vortex wandering. For each instantaneous velocity field, the vortex center is located by finding the point of lowest velocity magnitude. Then, all of the vector fields are aligned along their individual centers, and ensemble averaged. The $(\Delta Y, \Delta Z)$ origin of this vortex centered coordinate system follows the center of the neutral case vortex. The results in Fig. 12 are plotted in this coordinate system; however, one slight change is made. The vortex for the full span down case, in reality, is not centered at the same location as the neutral case vortex. To make it easier to compare the velocity and vorticity profiles, we have moved

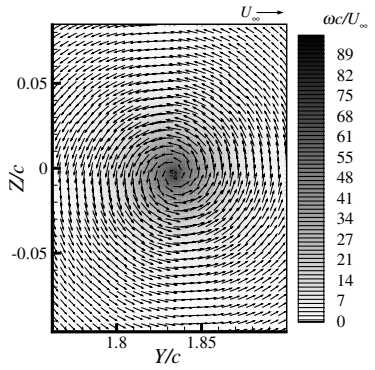

Fig. 11 Ensemble-averaged velocity and vorticity field for the neutral case at $X/c = 4.9$.

the center of the full span down case vortex to coincide with the neutral case vortex.

For the full span down case (dotted line) at all three streamwise positions shown in Fig. 12, the peak velocities in the vortex are increased by roughly 3–4%, and the peak vorticity is increased by roughly 11% with respect to the neutral case. For this case, we saw in the previous section that the MiTEs increment the spanwise loading distribution across the entire span, including near the root. According to lifting line theory, the amount of circulation that is left in the wake

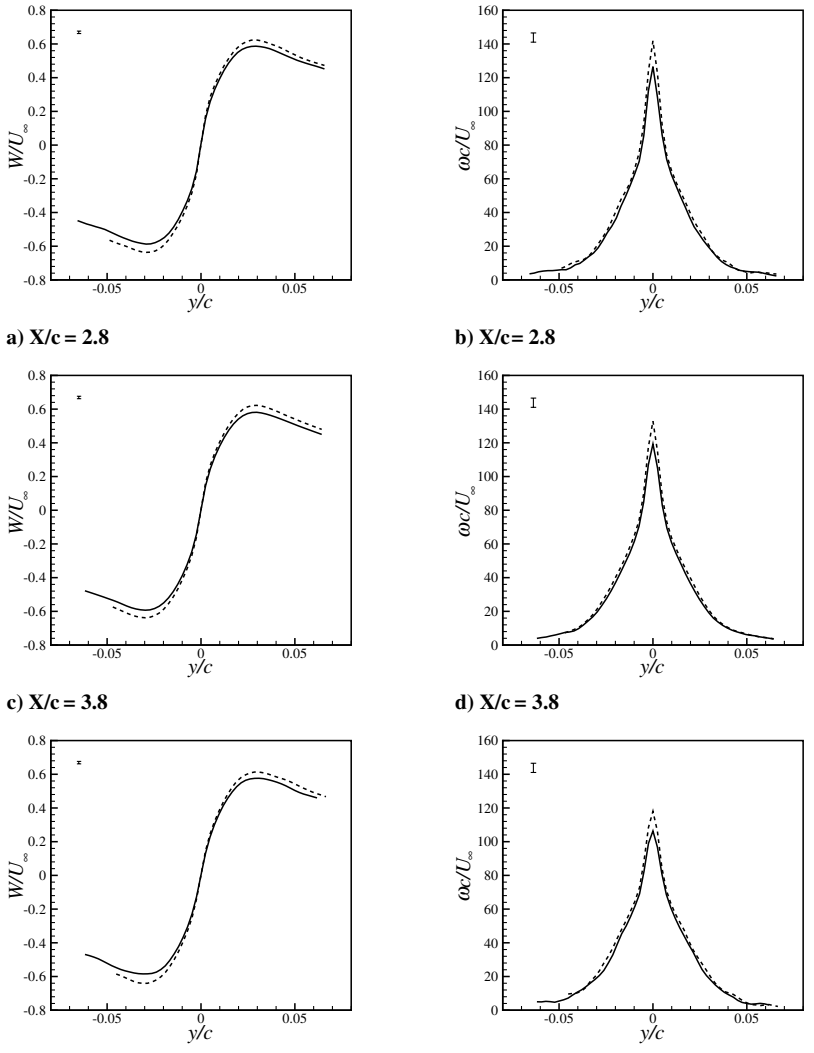

a) X/c = 2.8 **b) X/c= 2.8**

c) X/c = 3.8 **d) X/c = 3.8**

e) X/c = 4.9 **f) X/c = 4.9**

Fig. 12 Nondimensional velocity and vorticity profiles plotted in vortex centered coordinate system using center-averaging technique for the neutral case (solid line) and the full span down case (dotted line). The uncertainty is indicated by the bar shown in the top left corner of each plot.

of a wing is equal to the circulation at the root. Thus, it is not surprising that we see this increment in vorticity. Note also that as we move downstream, the vorticity peaks for both cases are falling as the vorticity in the core diffuses radially.

We look now at the same two cases measured over a much larger domain using a five-hole probe. Figure 13 compares the velocity profiles for the full span down and neutral cases (as with the PIV), and shows that intensification in tangential velocity occurs over this larger domain as well. This further demonstrates that MiTEs, when in the full span down configuration, increase the circulation about the wing. This also shows that the effect of the MiTEs can be felt in both the highly rotational region of the vortex (as in the PIV), as well as in the region further from the center, where vorticity levels are much lower. Aside from the increment in the vorticity profile and tangential velocity, the character of the vortex is essentially unchanged. Firstly, although not shown explicitly here, the five-hole probe measurements demonstrate that the streamwise velocity in the vortex is essentially uniform to roughly $\pm 4\%$ for all cases. Secondly, from the PIV, we see that the core is no more or less diffuse for either configuration, i.e., the vortex is equally coherent for both cases. Finally, the standard deviation of the instantaneous vortex center location from one image pair to another is comparable, i.e., the amount of vortex wandering never measurably changes.

Moving on to other flap configurations, in Fig. 14, we show the velocity profiles from the neutral case and three different configurations where $a_{\text{down}}/a = 0.13$. Although there are some observable differences between the velocity profiles, the change is quite small. This is not surprising given the small changes in the spanwise loading distribution that were shown in the preceding section. The same is true of the PIV results for these flap configurations.

Thus, for all a_{down}/a and Y_{flap}/a values examined, there is no change in how diffuse or concentrated the vortex is, or how much it wanders. Large a_{down}/a cases serve only to intensify the tangential velocity and vorticity while the general shape of the profiles is, essentially, preserved. For large and small actuation ratio cases, however, the mean location of the vortex does change significantly, and this is central to any active wake alleviation scheme. We now focus upon this.

We begin by examining the large a_{down}/a cases. The mean vortex center locations for the five large a_{down}/a cases are shown in Fig. 15. Results for all three streamwise locations are given on the same sets of axes, and the same data are plotted in both of the previously discussed coordinate systems. Figure 15a shows the vortex center location in physical space. For all cases, the vortex is generally moving in the inboard direction although the flap configuration clearly has an effect on the vortex center trajectory. Lower values of Y_{flap}/a cause the vortex to head upward, and higher values of Y_{flap}/a cause the vortex to head downward. In Fig. 15b, we present the same results in the $(\Delta Y, \Delta Z)$ coordinate system. Here, we see clearly that most of the authority we have over the vortex location is in the lift direction with respect to the neutral case vortex. The maximum lift

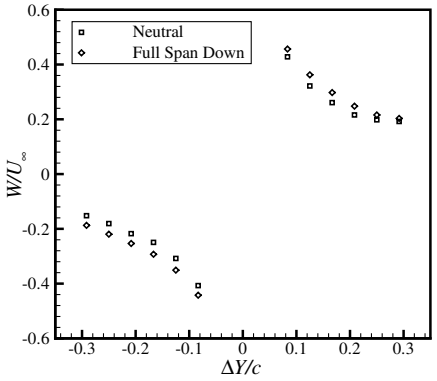

Fig. 13 Nondimensional velocity profiles from five-hole probe measurements plotted in vortex centered coordinate system. The uncertainty is smaller than the symbol size.

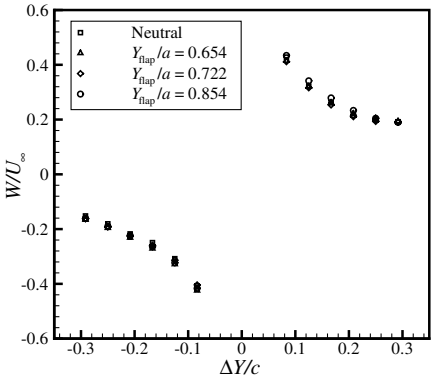

Fig. 14 Nondimensional velocity profiles from five-hole probe measurements plotted in vortex centered coordinate system for the neutral case and three cases where $a_{\text{down}}/a = 0.13$.

direction displacement at $X/c = 4.9$ is downward $0.028c$, and the maximum spanwise displacement is inboard $0.015c$.

The mean vortex center locations for seven configurations with $a_{\text{down}}/a = 0.13$ are given in Fig. 16 in the same coordinate systems as the large a_{down}/a cases. The only difference amongst these configurations is that Y_{flap}/a is varied from 0.119 to 0.854. Figure 16a shows that the vortex center trajectory is generally inboard for the neutral case and cases where Y_{flap}/a is less than 0.654. For the three cases where Y_{flap}/a is higher (MiTEs closer to the tip are actuated), we see that the path of the vortex is more severely altered. In Fig. 16b, we see a clear pattern in the path of the vortex due to the MiTEs with respect to the neutral case vortex. As we proceed further in the streamwise direction, we see a counterclockwise rotation and a radially expanding displacement. This demonstrates that the displacement of the vortex with respect to the neutral case position is growing as we proceed further in the streamwise direction, and the distance between vortex centers for neighboring MiTE configurations grows as well.

In terms of deflecting the vortex from its neutral case path, it is clear that the small a_{down}/a MiTE configurations have close to the same authority as the large a_{down}/a configurations. Large a_{down}/a cases produce deflections primarily in the lift direction whereas some small a_{down}/a cases produce large deflections in the spanwise direction. For small a_{down}/a cases, configurations with high Y_{flap}/a values produce large deflections; thus, they have more control authority over the vortex center position. The reason for this is likely because of the reduced spanwise influence associated with smaller a_{down}/a cases, as well as the ability to affect the loading distribution locally where its slope is most severe (near the tip). This allows the MiTEs to have more of an impact on the center of vorticity at the wing. The maximum spanwise displacement possible between two $a_{\text{down}}/a = 0.13$ cases is $0.041c$ at $X/c = 4.9$. This is achieved by the $Y_{\text{flap}}/a = 0.654$ and $Y_{\text{flap}}/a = 0.854$ cases, for which the difference in total lift experienced by the wing is only 0.91%. It may even be possible to eliminate the lift difference entirely through a more customized design of particular flap sizes. Therefore, by oscillating MiTEs between these two configurations, a relatively large displacement of the vortex center can be produced with very small lift variations.

IV. Conclusions

The results presented suggest that miniature trailing edge effectors can be used to introduce spatial disturbances to a trailing vortex in both the spanwise and lift directions. For cases where relatively large portions of the span are actuated down, the deflections are greater in the lift direction, whereas for cases where relatively small portions of the span are actuated down, the deflections are greater in the spanwise direction. The latter cases also carry with them the advantage of having a smaller effect on the total lift experienced by the wing. Contingent upon the dynamic effects, these spatial

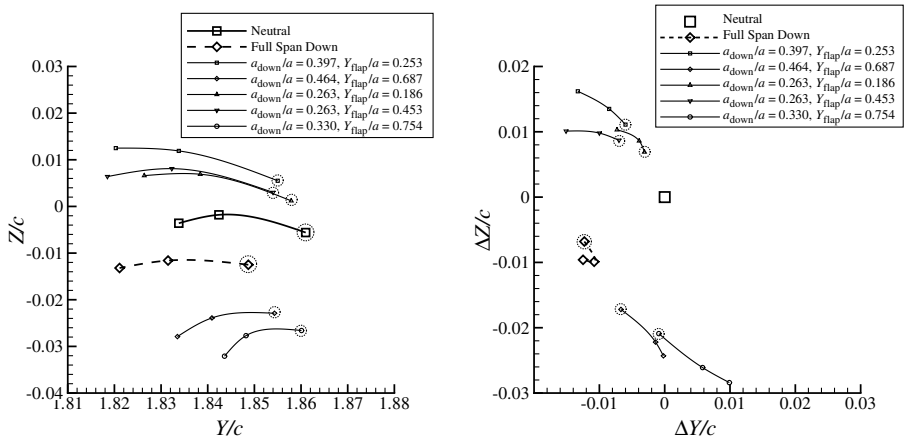

a) Uncentered coordinate system b) Centered coordinate system

Fig. 15 Mean vortex center locations measured by PIV for large a_{down}/a. The vortex location at $X/c = 2.8$ for each configuration is denoted by a dashed circle around the symbol. The uncertainty in both directions is indicated by the symbol size of the neutral case.

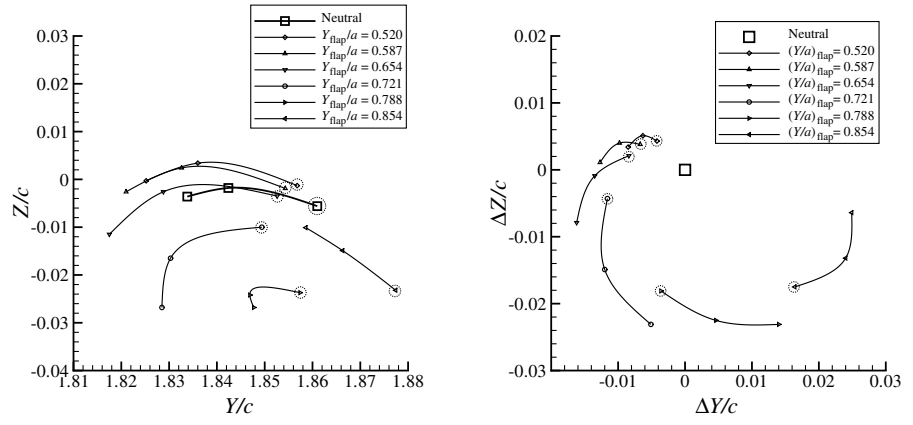

a) Uncentered coordinate system b) Centered coordinate system

Fig. 16 Mean vortex center locations measured by PIV for cases where $a_{down}/a = 0.13$. The vortex location at $X/c = 2.8$ for each configuration is denoted by a dashed circle around the symbol. The uncertainty in both directions is indicated by the symbol size of the neutral case.

disturbances can potentially be applied temporally in an active flow control scheme that may be useful for exciting vortex instability.

Acknowledgment

This work was performed with support from the Stanford Graduate Fellowship and the Stanford University Thermal and Fluid Sciences Affiliates Program.

References

[1] Liebeck, R. H., "Design of Subsonic Airfoils for High Lift," *Journal of Aircraft*, Vol. 15, No. 9, 1978, pp. 547–561.

[2] Neuhart, D. H., and Pendergraft, O. C., Jr., "A Water Tunnel Study of Gurney Flaps," NASA TM-4071, 1988.

[3] Storms, B. L., and Jang, C. S., "Lift Enhancement of an Airfoil Using a Gurney Flap and Vortex Generators," *Journal of Aircraft*, Vol. 31, No. 3, 1994, pp. 542–547.

[4] Giguére, P., Lemay, J., and Dumas, G., "Gurney Flap Effects and Scaling for Low Speed Airfoils," AIAA Paper 95-1881-CP, 1995.

[5] Myose, R., Heron, I., and Papadakis, M., "Effect of Gurney Flaps on a NACA 0011 Airfoil," AIAA Paper 96-0059, 1996.

[6] Jeffrey, D. R. M., and Hurst, D. W., "Aerodynamics of the Gurney Flap," AIAA Paper 96-2418-CP, 1996.

[7] Myose, R., Papadakis, M., and Heron, I., "Gurney Flap Experiments on Airfoils, Wings, and Reflection Plane Model," *Journal of Aircraft*, Vol. 35, No. 2, 1998, pp. 206–211.

[8] van Dam, C. P., and Yen, D. T., "Gurney Flap Experiments on Airfoils and Wings," *Journal of Aircraft*, Vol. 36, No. 2, 1999, pp. 484–486.

[9] Ross, J. C., Storms, B. L., and Carrannanto, P. G., "Lift-Enhancing Tabs on Multielement Airfoils," *Journal of Aircraft*, Vol. 32, No. 3, 1995, pp. 649–655.

[10] Ashby, D. L., "Experimental and Computational Investigation of Lift-Enhancing Tabs on a Multi-Element Airfoil," Ph.D. Thesis, Stanford Univ., Stanford, CA, 1996.

[11] Solovitz, S. A., "Experimental Aerodynamics of Mesoscale Trailing-Edge Actuators," Ph.D. Thesis, Stanford Univ., Stanford, CA, 2002.

[12] Solovitz, S. A., and Eaton, J. K., "Experimental Aerodynamics of Mesoscale Trailing-Edge Actuators," *AIAA Journal*, Vol. 40, No. 12, 2002, pp. 2538–2540.

[13] Solovitz, S. A., and Eaton, J. K., "Spanwise Response Variation for Partial-Span Gurney-Type Flaps," *AIAA Journal*, Vol. 42, No. 8, 2004, pp. 1640–1643.

[14] Bieniawski, S., "Distributed Optimization and Flight Control Using Collectives," Ph.D. Thesis, Stanford Univ., Stanford, CA, 2005.

[15] Widnall, S. E., "The Structure and Dynamics of Vortex Filaments," *Annual Review of Fluid Mechanics*, Vol. 7, 1975, pp. 141–165.

[16] Spalart, P. R., "Airplane Trailing Vortices," *Annual Review of Fluid Mechanics*, Vol. 30, 1998, pp. 107–138.

[17] Rossow, V. J., "Lift-Generated Vortex Wakes of Subsonic Transport Aircraft," *Progress in Aerospace Sciences*, Vol. 35, No. 6, 1999, pp. 507–660.

[18] White, R. P., and Balcerak, J. C., "An Investigation of the Mixing of Linear and Swirling Flows," Rochester Applied Science Associates, Inc. Report 72-04, Rochester, NY, 1972.

[19] Corsiglia, V. R., and Dunham, R. E., Jr., "Aircraft Wake-Vortex Minimization by Use of Flaps," NASA SP-409, 1976.

[20] Croom, D. R., "The Development and Use of Spoilers as Vortex Attenuators," NASA SP-409, 1976.

[21] Ortega, J. M., and Savaş, O., "Rapidly Growing Instability Mode in

Trailing Multiple-Vortex Wakes," *AIAA Journal*, Vol. 39, No. 4, 2001, pp. 750–754.
[22] Ortega, J. M., Bristol, R. L., and Savaş, O., "Wake Alleviation Properties of Triangular-Flapped Wings," *AIAA Journal*, Vol. 40, No. 4, 2002, pp. 709–721.
[23] Ortega, J. M., Bristol, R. L., and Savaş, O., "Experimental Study of the Instability of Unequal-Strength Counter-Rotating Vortex Pairs," *Journal of Fluid Mechanics*, Vol. 474, 2003, pp. 35–84.
[24] Graham, W. R., Park, S. W., and Nickels, T. B., "Trailing Vortices from a Wing with a Notched Lift Distribution," *AIAA Journal*, Vol. 41, No. 9, 2003, pp. 1835–1838.
[25] Durston, D. A., Walker, S. M., Driver, D. M., Smith, S. C., and Ömer Savaş, "Wake Vortex Alleviation Flow Field Studies," *Journal of Aircraft*, Vol. 42, No. 4, 2005, pp. 894–907.
[26] Crow, S. C., "Stability Theory for a Pair of Trailing Vortices," *AIAA Journal*, Vol. 8, No. 12, 1970, pp. 2172–2179.
[27] Crouch, J. D., "Instability and Transient Growth for Two Trailing-Vortex Pairs," *Journal of Fluid Mechanics*, Vol. 350, 1997, pp. 311–330.
[28] Rennich, S. C., "Accelerated Destruction of Aircraft Wake Vortices," Ph.D. Thesis, Stanford Univ., Stanford, CA, 1997.
[29] Rennich, S. C., and Lele, S. K., "Method for Accelerating the Destruction of Aircraft Wake Vortices," *Journal of Aircraft*, Vol. 36, No. 2, 1999, pp. 398–404.
[30] Crow, S. C., and Bate, E. R., Jr., "Lifespan of Trailing Vortices in a Turbulent Atmosphere," *Journal of Aircraft*, Vol. 13, No. 7, 1976, pp. 476–482.
[31] Bilanin, A. J., and Widnall, S. E., "Aircraft Wake Dissipation by Sinusoidal Instability and Vortex Breakdown," AIAA Paper 73-107, 1973.
[32] Crouch, J. D., Miller, G. D., and Spalart, P. R., "Active-Control System for Breakup of Airplane Trailing Vortices," *AIAA Journal*, Vol. 39, No. 12, 2001, pp. 2374–2381.
[33] Greenblatt, D., "Management of Vortices Trailing Flapped Wings via Separation Control," AIAA Paper 2005-61, 2005.
[34] Greenblatt, D., Pack-Melton, L. G., Yao, C.-S., and Harris, J., "Active Control of a Wing Tip Vortex," AIAA Paper 2005-4851, 2005.
[35] Spreiter, J. R., and Sacks, A. H., "The Rolling up of the Trailing Vortex Sheet and its Effect on the Downwash Behind Wings," *Journal of the Aeronautical Sciences*, Vol. 18, No. 1, 1951, pp. 21–32.

F. Coton
Associate Editor